RSC Advances

PAPER

View Article Online
View Journal | View Issue

Cite this: *RSC Adv.*, 2017, **7**, 23647

Enhanced selectivity in the conversion of glycerol to pyridine bases over HZSM-5/11 intergrowth zeolite†

Yuecheng Zhang, Xing Zhai, Hongyu Zhang and Jiquan Zhao *

A composite co-crystalline zeolite HZSM-5/11(78) was synthesized and tested in the conversion of glycerol with ammonia to pyridine bases (pyridine, 2-methylpyridine, 3-methylpyridine). The HZSM-5/11(78) showed good performance compared to other zeolites with similar Si/Al ratios such as HZSM-5(80), HZSM-11(80) and the physical mixture of HZSM-5(80) and HZSM-11(80). Characterization results from the N_2 adsorption–desorption and IR of the adsorbed pyridine indicated that the good performance of HZSM-5/11(78) was related to the higher surface area and co-existence of an appropriate ratio of Lewis and Brønsted sites, which are derived from the intergrowth between zeolites HZSM-5 and HZSM-11. The parameters affecting the catalytic performance of HZSM-5/11(78) were investigated systematically. The optimal conditions for producing pyridine bases from glycerol with ammonia over this catalyst were determined, including a reaction temperature of 520 °C, 0.1 MPa pressure with a molar ratio of ammonia to glycerol of 12 : 1, and a GHSV of 300 h^{-1}.

Received 24th February 2017
Accepted 23rd April 2017

DOI: 10.1039/c7ra02311a

rsc.li/rsc-advances

1. Introduction

Driven by the increasing energy demand and awareness of the environment, more attention has been paid to replace fossil fuel resources with renewable bioenergy. Biodiesel has become one of the most feasible alternatives to reduce consumption of diesel from crude oil because of its environmental benefits and renewable nature. Biodiesel is easily manufactured by transesterification of triglycerides with methanol catalyzed by an acid or base catalyst. Generally about 100 kg of crude glycerol as a co-product is generated for one ton of biodiesel produced.[1,2] With the rapidly growing consumption of biodiesel, glycerol has become available in large excess, which leads to a big decrease in its price in the world market. Therefore, conversion of glycerol into value-added chemicals is urgent to help sustainable development of the biodiesel industry. Various efforts have been made to transform glycerol into commercially valued products, such as acetonitrile, propionitrile, pyridine, acrolein, lactic acid, 1,2-propanediol, 1,3-propanediol and ethylene glycol.[3–6] The double dehydration of glycerol to acrolein has been the most investigated, and has been realized over an ocean of acid catalysts.[7–17]

It is well known that acrolein is a raw material or a key intermediate in the synthesis of pyridine bases over HZSM-5 based catalysts.[18–21] Pyridine bases (pyridine, 2-methylpyridine, 3-methylpyridine and 4-methylpyridine) are not only widely used in synthetic rubber and dye, but also can be used in medicine and pesticide production. Therefore, conversion of glycerol to pyridine bases is feasible theoretically, and valuable from the point of view of the conversion of glycerol to value-added chemicals. In fact, several decades ago Cullinane[22] already found the formation of pyridine by heating glycerol and ammonia or urea in contact with alumina and aluminium silicates. Very recently, the synthesis of pyridine bases from glycerol has been realized in moderate yields by several groups including us. Güllü and his coworkers[23] reported that 3-methylpyridine and pyridine were obtained in a yield as high as 68% from glycerol and ammonium hydrogen phosphate $(NH_4)_2HPO_4$ in an acidic medium by thermal conversion reactions under microwave irradiation. However, this protocol is of difficulty in implement in large scale production. Recently, Xu *et al.*[5] performed the conversion of glycerol to pyridine bases in a total yield of 35.6% over HZSM-5(25) in a fixed-bed reactor. Using this protocol pyridine bases can be synthesized continuously from glycerol and ammonia, however, the yield of pyridine bases is not satisfactory. We improved the catalysis of HZSM-5 by doping copper into the matrix of HZSM-5, the total yield of pyridine bases reached up to 42.8% over the catalyst 4.6% Cu/HZSM-5(38).[6] Characterization results revealed that the doping of copper into HZSM-5 led to an appropriate proportion of Lewis and Brønsted sites, which is important to determine the total selectivity of pyridine bases. The results suggest that the catalytic performance of HZSM-5 in the conversion of glycerol to pyridine bases could be improved by regulating its acidity and

School of Chemical Engineering and Technology, Hebei University of Technology, Tianjin 300130, PR China. E-mail: zhaojq@hebut.edu.cn; Fax: +86 22 60202926; Tel: +86 22 60202926

† Electronic supplementary information (ESI) available. See DOI: 10.1039/c7ra02311a

pore structure. This inspired us to pursue alternative routes relying on different zeolite frameworks, rather than metal doping.

Composite co-crystalline zeolite HZSM-5/11, which is a promising zeolite for industrial application,[24–26] may have suitable acidity and pore structure for converting glycerol to pyridine bases. This zeolite is a co-crystalline porous tectosilicate, that is a three-dimensional framework of silicate tetrahedra with SiO_2, comprising an intergrowth between zeolites HZSM-5 and HZSM-11.[27] Therefore, a co-crystalline zeolite HZSM-5/11(78) was synthesized and tested in the conversion of glycerol with ammonia to pyridine bases in a fix-bed reactor. The catalytic results indicated that the co-crystalline zeolite HZSM-5/11(78) had good performance compared to other zeolites such as HZSM-5(80), HZSM-11(80) and the physical mixture of HZSM-5(80) and HZSM-11(80) known as HZSM-5/HZSM-11(80). Characterization results disclosed the reasons leading to the enhanced selectivity towards pyridines of HZMS-5/11(78).

2. Experimental section

2.1 Materials and catalysts

The reagents used to prepare the zeolites were obtained from KRS Chemical Reagent Cooperation, Tianjin, China.

HZSM-5(80) was provided by Nankai University Catalyst Plant, Tianjin, China. HZSM-11(80) was purchased from Shen Tan Environmental Protection New Materials Plant, Shanghai, China. HZSM-5/HZSM-11(80) was prepared by direct mixing HZSM-5(80) with HZSM-11(80) in a weight ratio of 60 to 40. The data in the parentheses of the text refer to the Si/Al ratio in the zeolites.

Composite co-crystalline zeolite HZSM-5/11(78) was synthesized by using the reported method.[27] NaOH (Fisher, 3.25 g) and meteorological silica (Fisher, 37.5 g) were added to distilled water (160 ml) with strong stirring to give a solution (solution 1). $NaAlO_2$ (Fisher, 0.75 g) and tetrabutylammonium bromide (Aldrich, 10 g) were added to distilled water (30 ml) with vigorous stirring to generate another clear solution (solution 2). Solution 2 was added dropwise to solution 1 under stirring. Then, the slurry was transferred into an autoclave, and held at 163 °C for 72 h with stirring for crystallization. After crystallization, the mixture was cooled to room temperature then filtered. The filter cake was washed with distilled water thoroughly until the pH closed to neutral. The obtained solid was dried at 110 °C for 12 h and calcined at 550 °C for 6 h in the muffle furnace (temperature ramp 20 °C min^{-1}). The solid was stirred in 1 M solution of NH_4NO_3 (8 ml per gram of solid powder) for 2 h at 90 °C with stirring, then cooled and filtered. This ion exchange was repeated 3 times. Then the solid was washed with distilled water until no free nitrate ion was detected. Finally, the solid collected was dried at 110 °C for 12 h, calcined at 550 °C for 6 h (temperature ramp 20 °C min^{-1}).

The catalysts (HZSM-5, HZSM-11, HZSM-5/11 and HZSM-5/HZSM-11) were prepared by the kneading extruding method. As an example, the HZSM-5/11(78) catalyst was prepared as the following procedures: 6 g of γ-Al_2O_3 was added in a beaker, and a suitable amount of 5% dilute nitric acid was added to form alumina sol, then 24 g of HZSM-5/11(78) was added to the solution. The mixture was kneaded for 2 h in a kneader and the resulting kneaded material was processed in an extruder to obtain extrudates with a diameter of 2 mm and a length of 2.5 mm. The catalyst precursor was dried at 110 °C for 6 h and calcined at 550 °C for 6 h to yield the catalyst.

2.2 Characterization of catalysts

Elemental compositions (mainly the bulk SiO_2/Al_2O_3 molar ratio) of the zeolites were determined by a Rigaku ZSX Primus II X-ray fluorescence (XRF) spectrometer.

X-ray diffraction spectroscopy (XRD) was carried out with a Rigaku D/max 2500 X-ray diffractometer with Cu Kα radiation in the 2θ range of 5–50° and scanning the tube voltage 40 kV, the current 20 mA.

The morphology and particle size distribution of the zeolite samples were taken on an FEI Nova nano SEM450 field-emission scanning electron microscope at different accelerating voltages. The samples were uniformly dispersed onto the conductive double-sided adhesive posted on copper.

The IR spectra of adsorbed pyridine were performed with a Thermo Nicolet Nexus 470 spectrometer. Ground samples of the zeolites were pressed onto self-supporting wafers with a diameter of 20 mm and a weight of 30 mg. The wafers were heated at 400 °C under a vacuum of 5×10^{-5} Pa for 1 h to remove the physisorbed water molecules, then the samples were cooled to 200 °C. Pyridine was adsorbed at the temperature for 15 min. Then the cell was evacuated at 200 °C for 1 h under a high vacuum of 5×10^{-5} Pa to remove the physisorbed pyridine molecules on the wafers. The IR spectra were recorded on the computer.

Nitrogen adsorption–desorption was conducted at the temperature of 77 K, using a Micromeritics ASAP 2020 apparatus. The specific surface area was calculated by the BET equation and the pore volume was calculated at a relative pressure of $P/P_0 \approx 0.99$, assuming full surface with nitrogen.

The NH_3-TPD tests were performed on a Micromeritics Auto Chem II-2920. In the test about 100 mg of sample was placed in a reaction tube and pre-treated at 400 °C for 1 h under an argon flow of 50 ml min^{-1}. After cooling to 100 °C under the argon flow, ammonia adsorption was performed to the reaction tube. After the catalyst surface became saturated, the ammonia was eliminated by flowing argon for 1 h at 100 °C. TPD measurement was carried out from 100 °C to 600 °C. The amount of desorbed NH_3 was measured by an on-line gas chromatograph.

2.3 Catalytic tests

The catalytic tests were run in a fixed-bed reactor (inner diameter = 20 mm, length = 1000 mm). About 15 ml of the catalyst was charged in the middle of the reactor to build a catalyst zone of about 48 mm, while both ends of the reactor were filled with Pyrex glass chips. The fixed-bed reactor was placed in an electric furnace equipped with four temperature controllers. The reaction temperature was measured by a thermocouple inserted in the center of the catalyst sample. During the catalytic run, an

aqueous solution of 20 wt% glycerol and ammonia was pumped into a vaporizer (approximately 300 °C), in which the two reactants were preheated and mixed, then the vaporized mixture was fed into the reactor. Liquid and gaseous products were separated by passing through a gas–liquid separator and the liquid products were condensed in an ice-water trap. The gaseous products were collected after passing through an absorber with water to remove the entrained liquid products of low boiling point for analysis. The components of the collected reaction mixture were identified using a GC-MS (HP5971 GC-MS) equipped with a 30 m SE-30 capillary column. The organic products were pyridine, 2-picoline, 3-picoline, acetonitrile, propionitrile, acetaldehyde, coke, C_2H_4 and C_3H_6.

The quantitative analysis of the products was carried out on a gas chromatograph equipped with a 30 m SE-54 capillary column using *n*-butanol as an internal standard. The GC temperature program was set to 80 °C for 8 min, and 40 °C min^{-1} up to 200 °C. The contents of the gaseous products, except for carbon dioxide (CO_2), were determined by the external standard method.

The contents of CO_2 was collected in the form of ammonium carbonate, and was tested by a titration method [ISO 3422-1975 (E)].[4]

$$\text{Glycerol conversion } (\%) = \frac{\text{moles of glycerol reacted}}{\text{moles of glycerol fed}} \times 100\%$$

$$\text{Product yield } (Y\%) = \frac{\text{moles of carbon in the product}}{\text{moles of carbon in glycerol fed}} \times 100\%$$

$$\text{Carbon balance } (C\%) = \frac{\text{total of moles of carbon in the products}}{\text{moles of carbon in glycerol fed}} \times 100\%$$

3. Results and discussion

3.1 Catalysis of zeolites in the conversion of glycerol to pyridine bases

The main objective of this study is to find a catalyst with high selectivity to convert glycerol with ammonia to pyridine bases. The synthesized zeolite was first characterized by XRD and XRF, and confirmed to be HZSM-5/11(78). The detailed characterization results will be described latter. The sample of HZSM-5/11(78) was then subject to catalytic test under different reaction conditions.

3.1.1 The effect of temperature on the synthesis of pyridine bases from glycerol. The effect of the reaction temperature on the catalytic test of HZSM-5/11(78) was first investigated in the temperature from 300 °C to 540 °C under 0.1 MPa by maintaining the molar ratio of ammonia to glycerol at 9 : 1 and a GHSV of 700 h^{-1}. The results are shown in Fig. 1. As observed from Fig. 1, the conversion of glycerol increased with the increase of the reaction temperature from 300 °C to 480 °C, and reached up to 100% at 480 °C. When the temperature was higher than 480 °C, the conversion of glycerol was always 100%.

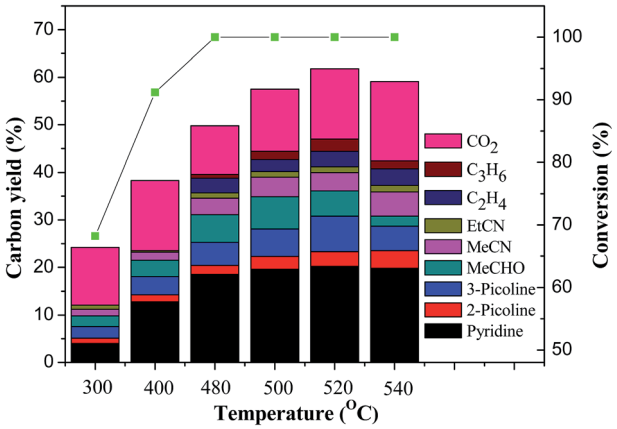

Fig. 1 Effect of reaction temperature on the performance of the HZSM-5/11(78) catalyst. The line above the columns refers to the conversion of glycerol. Reaction conditions: ammonia/glycerol molar ratio 9 : 1, atmospheric pressure, GHSV 700 h^{-1}, time on stream 2 h. 20 wt% glycerol aqueous solution.

Meanwhile, the total yield of pyridine bases increased with the temperature from 300 °C to 520 °C and reached a maximum of 30.8% at 520 °C. With further increase of the reaction temperature, the total yield of pyridine bases decreased instead. For instance, the total yield of pyridine bases was 28.7% at 540 °C. High temperature was in favor of the formation of ethylene, acetonitrile and carbon dioxide, which led to the decrease of the selectivity towards the pyridine bases. The optimal temperature was 520 °C from the view point of total yield of pyridine bases, which was same as that of the reaction over 4.6% Cu/HZSM-5 catalyst,[6] higher than the ones for the synthesis of pyridine bases from other raw materials.[15,16,18,20,28–32] The high temperature in the synthesis of pyridine bases from glycerol compared to other feed stocks can be attributed to the high energy requirement for the generation of acetaldehyde of and formaldehyde from acetol and 3-hydroxypropanal. Acetaldehyde and formaldehyde are also key intermediates in the transformation of glycerol to pyridine bases in addition to acrolein.[6]

3.1.2 The effect of the molar ratio of ammonia to glycerol on the reaction. The influence of the molar ratio of ammonia to glycerol on the reaction was investigated in the range of 6 : 1 to 18 : 1 under 0.1 MPa of ammonia pressure and GHSV of 700 h^{-1} at 520 °C. As shown in Fig. 2, the conversion of glycerol was kept at 100% in all cases. The total yield of pyridine bases increased with the increase of the molar ratio of ammonia to glycerol initially, and reached its maximum of 33.1% at the molar ratio of 12 : 1, then decreased gradually with further increase of the molar ratio of ammonia to glycerol. The excessive amount of ammonia not only can accelerate acrolein and acetaldehyde with ammonia to form imines, which are important intermediates to form acetonitrile, but also can weaken the acidity of the HZSM-5/11 catalyst. As can be seen in Fig. 2, excessive molar ratio of ammonia to glycerol can push the conversion of acetaldehyde, an intermediate derived from glycerol, to acetonitrile. Meanwhile, the selectivity towards ethylene always increased with the increase of the molar ratio of ammonia to glycerol. It

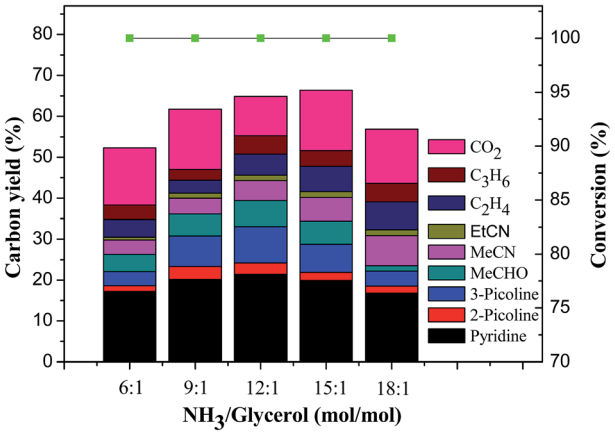

Fig. 2 Effect of the molar ratio of ammonia to glycerol on the performance of the HZSM-5/11(78) catalyst. The line above the columns refers to the conversion of glycerol. Reaction conditions: reaction temperature 520 °C, atmospheric pressure, GHSV 700 h^{-1}, time on stream 2 h, 20 wt% glycerol aqueous solution.

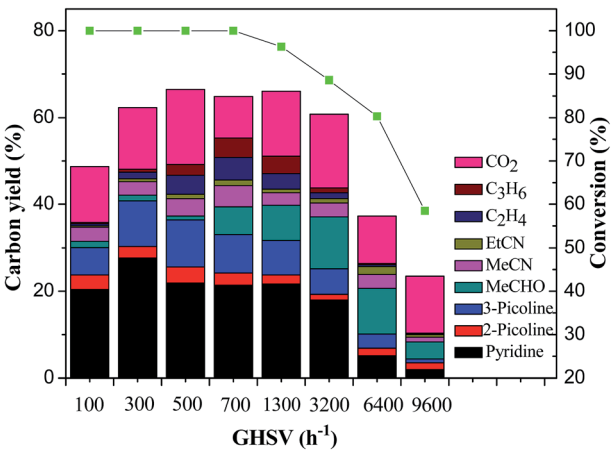

Fig. 3 Effect of GHSV on the performance of the HZSM-5/11(78) catalyst. The line above the columns refers to the conversion of glycerol. Reaction conditions: reaction temperature 520 °C, ammonia/glycerol molar ratio 12 : 1, atmospheric pressure, time on stream 2 h. 20 wt% glycerol aqueous solution.

was concluded that the optimal molar ratio of ammonia to glycerol was 12 : 1 for the synthesis of pyridine bases from glycerol over HZSM-5/11(78).

3.1.3 The effect of GHSV on the conversion of glycerol to pyridine bases. GHSV is a key parameter in the catalytic reactions running in a fixed-bed reactor. Thus, the influence of GHSV on the conversion of glycerol to pyridine bases over HZSM-5/11(78) was screened under 0.1 MPa ammonia pressure, and the molar ratio of ammonia to glycerol of 12 : 1 at 520 °C. The results are shown in Fig. 3. Because Low GHSV equals long residence time of the reactants on the catalyst, the conversion of glycerol was maintained at 100% in the cases of GHSV less than 700 h^{-1}. With the increase of GHSV from 700 h^{-1} to 9600 h^{-1}, the conversion of glycerol decreased from 100% to 58.3%. The total yield of pyridine bases increased from 30.1% to 40.8% as the GHSV increased from 100 h^{-1} to 300 h^{-1}, and then decreased gradually with further increase of GHSV. Very low GHSV led to oligomerization of the intermediates such as aldehyde and the imines generated in the reaction, enhancing the carbon deposition on the catalyst, which was the main reason for the very low carbon balance at the GHSV of 100 h^{-1}. At extremely high GHSV of 9600 h^{-1}, the conversion of glycerol was only 58.3% and the total yield of pyridine bases was only 3.4% due to the short residence time of the reactants on the catalyst.

3.1.4 The influence of water content of aqueous glycerol solution in the conversion of glycerol to pyridine bases. Previous investigation[5,6] disclosed that water content in the aqueous glycerol solution had obvious effect on the transformation of glycerol to pyridine bases over HZSM-5 based catalysts. Thus, the effect of water content on the reaction was screened by using aqueous glycerol solutions with different water contents as raw materials. The results are summarized in Table 1. As can be seen the conversion of glycerol increased with water content in the feed increased from 0% to 70%, and was maintained at 100% in the cases of water content above 70%. Both the yields of pyridine and 3-picoline increased with the increase of water content, and reached to their maxima at the water content of 80%, which led to the highest total yield of pyridine bases of 40.8%. The result is very different with the one of the same reaction over HZSM-5(25) catalyst reported by Xu *et al.*,[5] in which the total yield of pyridine bases decreased with the increase of water content. In our experiments, it was observed that low water content in the feed will led to severe carbon deposition, and increased the deactivation rate of the catalyst HZSM-5/11(78). Similar results were also discovered in

Table 1 The influence of water content in the conversion of glycerol to pyridine bases[a]

		Selectivity (%)										
H_2O (%)	Conv (%)	py	2-pic	3-pic	MeCN	EtCN	MeCHO	C_2H_4	C_3H_6	CO_2	*Y* (%)	*C* (%)
90	100	15.5	3.6	5.5	4.8	0.9	1.1	2.9	2.7	14.3	24.6	51.3
80	100	27.7	2.6	10.5	3.1	0.7	1.3	1.5	0.7	14.2	40.8	62.3
70	100	20.9	2.9	6.9	3.4	0.3	1.9	2.7	2.4	10.4	30.7	52.2
60	98.2	16.6	2.9	6.6	2.8	0.9	0.4	5.1	3.1	6.1	26.1	45.4
40	97.3	8.4	2.0	4.0	2.6	0.8	0.2	10.3	14.7	6.5	14.4	50.9
0	97.0	3.7	0.6	1.1	0.9	0.2	0.9	8.6	9.3	5.8	5.4	33.2

[a] py: pyridine; 2-pic: 2-picoline; 3-pic: 3-picoline; *C*: carbon balance. *Y*: total yield of pyridine, 2-picoline and 3-picoline. Reaction conditions: HZSM-5/11(78) catalyst, reaction temperature 520 °C, ammonia/glycerol molar ratio 12 : 1, atmospheric pressure, GHSV 300 h^{-1}, time on stream 2 h.

the catalytic conversion of glycerol to acrolein,[33,34] and the synthesis of pyridine bases from other feed stocks.[35] However, when the water content was higher than 80%, the selectivity towards pyridine and 3-picoline decreased sharply. This might be ascribed to the competition of excessive water with glycerol on the acid sites of the catalyst,[36] which affects the acidity of the catalyst. The acidity of the catalyst is a key factor to influence the catalysis of the catalyst in the conversion of glycerol to pyridine bases.[6]

From the systematic investigation of parameters affecting the catalytic performance of HZSM-5/11(78), the optimal conditions for producing pyridine bases from glycerol with ammonia over this catalyst were achieved, including a reaction temperature of 520 °C, 0.1 MPa pressure with a molar ratio of ammonia to glycerol of 12 : 1, a GHSV of 300 h^{-1} and glycerol concentration in water of 20%. Under the optimal conditions the total carbon yield of pyridine basses was maintained at 40.8% in the first 16 h, then the catalyst deactivated gradually, and the total yield of pyridine basses was about 28.6% after the catalyst was on stream of 32 h.

3.1.5 Comparison of HZSM-5/11(78) with other zeolites. From the above investigation, the optimal reaction conditions for the conversion of glycerol to pyridine bases over HZSM-5/11(78) were obtained, which were: molar ratio of NH_3 to glycerol, 12 : 1; atmospheric pressure; reaction temperature, 520 °C; and GHSV, 300 h^{-1}; glycerol concentration, 20%. Under the optimal reaction conditions the performance of HZSM-5/11(78) was compared with those of other zeolites including HZSM-5(80), HZSM-11(80) and the physical mixture of HZSM-5(80) and HZSM-11(80) in a similar ratio of the two components in HZSM-5/11(78). The results are shown in Table 2. In view of the total yield of pyridine bases, HZSM-5/11(78) performed best among the tested zeolites; HZSM-11(80) gave the worst result in the contrary. Though the second highest total yield of pyridine bases was received over HZSM-5(80), it was much lower than that over HZSM-5/11(78). Besides, the total yield of pyridine bases over HZSM-5/HZSM-11(80) was between the ones over HZSM-5(80) and HZSM-11(80). The results indicate that the co-crystalline structure and physical characteristics of HZSM-5/11(78) have benefit effect on the conversion of glycerol to pyridine bases.

3.1.6 Pathways for product formation. For screening the pathway of glycerol conversion to pyridine bases, the reaction was run at high GHSV to keep low glycerol conversion, respectively. Under low glycerol conversion, some intermediates could be detected. Herein, the reaction was run at high GHSV of 3200 h^{-1}, and the composition of the reaction mixture was analyzed by GC-MS (Fig. S4†). In the mixture, some primary intermediates such as allyl alcohol, acetaldehyde, and *N*-methylene ethanamine, were observed besides the final products. The intermediates disclosed here are same as or similar to the ones detected in the conversion of glycerol to pyridine bases over the catalyst 4.6% Cu/HZSM-5(38).[6] According to the principles of organic reactions, the formation pathways of the primary intermediates can be proposed. As shown in Scheme 1, glycerol was firstly converted into 3-hydroxy propanal (3-HPA) or acetol by the eliminating one H_2O over the catalyst. The generated 3-hydroxy propanal was dehydrated to acrolein, and converted into acetaldehyde and formaldehyde through retro-aldol condensation. Acetol can be decomposed to acetaldehyde.

Table 2 The conversion of glycerol with ammonia over various catalysts to pyridine bases[a,b]

		Selectivity (%)										
Catalyst	Conv (%)	py	2-pic	3-pic	MeCN	EtCN	MeCHO	C_2H_4	C_3H_6	CO_2	*Y* (%)	C^c (%)
HZSM-5(80)	100	19.9	1.8	8.7	3.8	1.6	2.7	1.2	0.5	16.1	30.4	61.3
HZSM-11(80)	100	14.4	2.0	4.8	3.0	0.9	1.9	2.4	0.8	10.5	21.2	40.7
HZSM-5/11(78)	100	27.7	2.6	10.5	3.1	0.7	1.3	1.5	0.7	14.2	40.8	62.3
HZSM-5/HZSM-11(80)	100	17.8	3.1	6.2	3.9	0.9	1.0	3.8	2.1	15.8	27.1	54.6

[a] Reaction conditions: reaction temperature 520 °C, ammonia/glycerol molar ratio 12 : 1, atmospheric pressure, GHSV 300 h^{-1}, time on stream 2 h. 20 wt% glycerol aqueous solution 0.05 ml min^{-1}, NH_3 29.2 ml min^{-1}. [b] py: pyridine; 2-pic: 2-picoline; 3-pic: 3-picoline; *C*: carbon balance. *Y*: total yield of pyridine, 2-picoline and 3-picoline. [c] The carbon balance is the sum of the carbon of the quantitatively analyzed products, not involving the carbon in the coke.

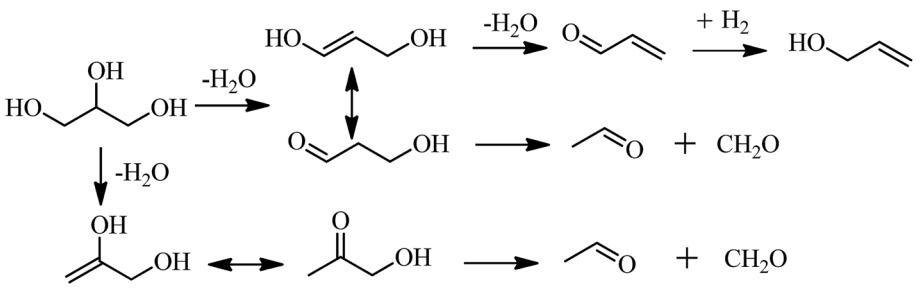

Scheme 1 Pathways for the dehydration of glycerol to aldehydes.

Once the formation of the primary intermediates, they condensed readily with ammonia over the catalyst to generate the corresponding imines, which are not detectable due to their instability. Finally, the intermediate imines were transformed to pyridine bases over the HZSM-5/11 catalyst as shown in Scheme 2.[5,6]

3.2 Characterization of the catalysts

The sample of the expected composite co-crystalline zeolite HZSM-5/11 was firstly subjected to the X-ray fluorescence analysis, from which it was found that the Si/Al ratio in the sample is 78 : 1 (Fig. S1†). Therefore, the synthesized zeolite was known as HZSM-5/11(78).

The XRD was employed to confirm the successful synthesis of composite co-crystalline zeolite HZSM-5/11(78). Fig. 4A shows the XRD patterns of the fresh zeolites and the used HZSM-5/11(78). As shown in Fig. 4A(a), HZSM-5(80) has the typical MFI structure. The XRD patterns of HZSM-5(80) at 2θ range of 20–25° have five peaks and two obvious peaks at 2θ range of 45–46°. The XRD patterns of HZSM-11(80) show two peaks at 2θ range of 20–25° and only one peak at 2θ range of 45–46° (Fig. 4B). These are the main differences between HZSM-5(80) and HZSM-11(80) from the XRD profiles. By comparing the pattern features in Fig. 4A(a, b and e), it is clear that the patterns of HZSM-5/HZSM-11(80) are just the superposition of those of HZSM-5(80) and HZSM-11(80). The peak at 2θ of 24.4° is clearly observed, which is the key feature of a physical mixture of HZSM-5(80) and HZSM-11(80). As shown in Fig. 4A(c), the XRD patterns of HZSM-5/11(78) show consistency with the expected reflections in the literature.[37,38] There is MEL phase in HZSM-5/11(78) intergrowth zeolites besides the MFI phase. This can be obtained by comparing the XRD patterns of the samples of HZSM-5(80) HZSM-5/11(78). The evidences are the strong decrease of the intensity of the reflections (051) and (303), and the disappearance of the reflection (133) in the XRD patterns of HZSM-5/11(78) compared with those of HZSM-5(80).[27] A further evidence of HZSM-5/11(78) intergrowth zeolite is the peak at 2θ of 45.5°.

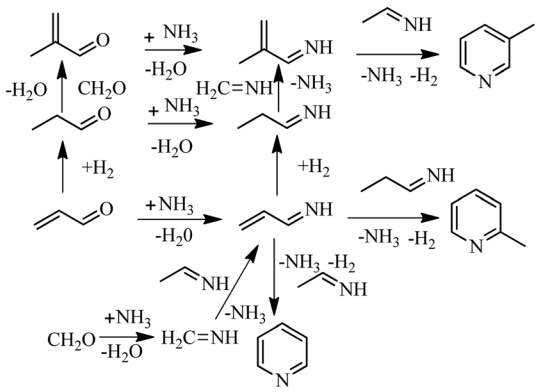

Scheme 2 Possible pathways for the formation of pyridine bases.

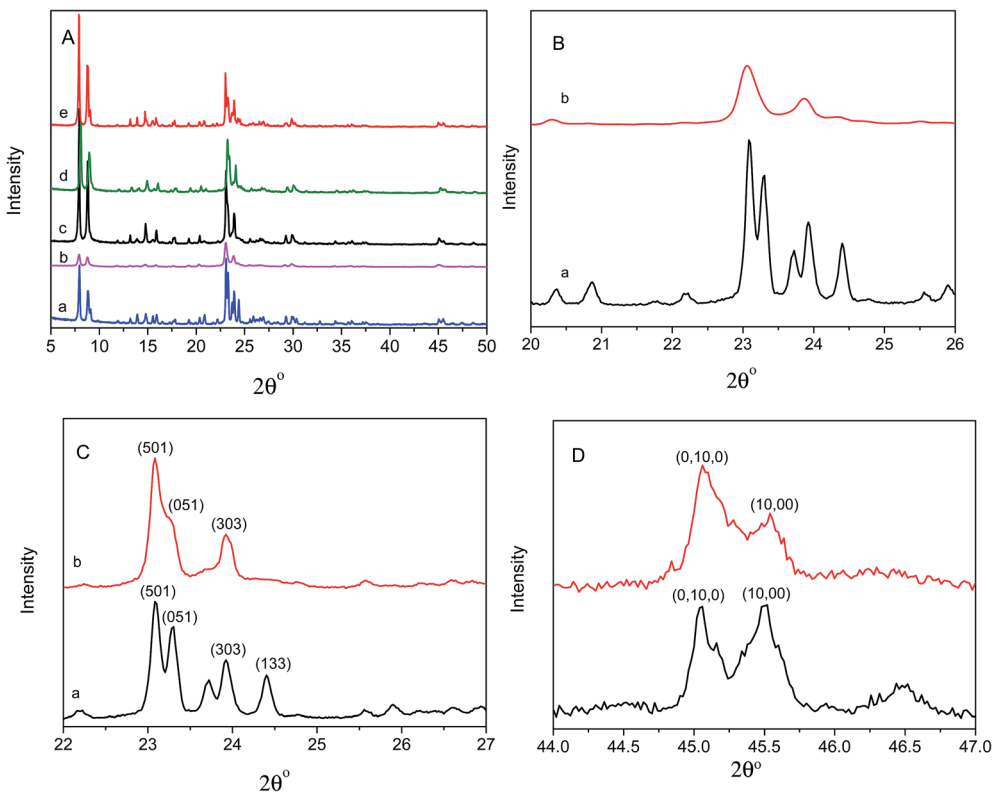

Fig. 4 (A) XRD patterns of the catalyst samples. (a) HZSM-5(80); (b) HZSM-11(80); (c) HZSM-5/11(78)(fresh); (d) HZSM-5/11(78)(used); (e) HZSM-5/HZSM-11(80). (B) XRD patterns of the catalyst samples. (a) HZSM-5(80); (b) HZSM-11(80). (C) XRD patterns of the catalyst samples. (a) HZSM-5(80); (b) HZSM-5/11(78). (D) XRD patterns of the catalyst samples. (a) HZSM-5(80); (b) HZSM-5/11(78).

In the patterns of pure HZSM-5(80) the peak at 2θ of 45.5° is always clearly observed, while in the patterns of intergrowth zeolite HZSM-5/11(78) this peak is strongly diminished (Fig. 4D), which is in accord with the presence of the MEL framework of HZSM-11 intergrowth into the MFI structure.[27,39] The contribution of MFI and MEL structure can be estimated from the X-ray powder patterns. The relative amount of HZSM-5 to HZSM-11 in the intergrowth zeolite is 60 : 40, calculated using the relative height of the reflections (0, 10, 0) and (10, 0, 0) of the samples of ZSM-5 and ZSM-5/11 at 2θ range of 45–46°.[40]

Fig. 4A(c and d) shows the XRD patterns of the samples of the fresh and used HZSM-5/11(78). No obvious difference was observed between the XRD patterns of the two samples, which indicated the framework of HZSM-5/11(78) was stable under the catalytic conditions.

Due to the fact that the crystallite size and zeolite morphology can affect the catalytic activity in catalytic reactions,[41,42] the morphology and crystallite size were investigated by using scanning electron microscopy, and are shown in Fig. 5. The HZSM-5(80) zeolite (Fig. 5a) exhibits hexagon morphology with an average length of 1.5 μm, while the HZSM-11(80) zeolite (Fig. 5b) has spherical morphology with a diameter from 0.3–0.8 μm. In addition, the surface of the spherical aggregates of HZSM-11 is covered with micro holes.

The presented HZSM-5/11(78) (Fig. 5c) shows twinned hexagon crystal morphology, having intergrowth phase, and an average length of 1.5 μm. This type of morphology can also be described as coffin shaped crystallography (inset Fig. 5c) with pyramidal appearance at (010) face consisting of self assembled intergrowth components. Such crystals have been reported mainly for HZSM-5 as well as for some cases of HZSM-5/11 composite.[26,43–45] However, the SEM image of HZSM-5/HZSM-11(80) (Fig. 5d) exhibits a simple mixture of the hexagon crystals of HZSM-5 and spherical aggregates of HZSM-11. The SEM images confirm that HZSM-5/11(78) is a co-crystalline zeolite.

The porous structure and specific surface areas of the fresh zeolites and the used HZSM-5/11(78) were determined by N_2 adsorption–desorption. The results are summarized in Table 3. All the samples showed type IV isotherms, indicating the existence of mesopores in the catalysts (Fig. S2A and B†). The specific surface areas of the fresh zeolites are in order of HZSM-5/11(78), HZSM-5(80), HZSM-5/HZSM-11(80) and HZSM-11(80), which is just consistent with the order of the total yield of pyridine bases over them as shown in Table 2. The combined results indicated that the bigger the specific surface areas of the zeolite are, the higher the total yield of pyridine bases over the zeolite is received. The increase of the specific surface area not only facilitates the contact between reactive molecules, but also can accommodate more coke formed. It seems that the carbon balance is also in line with the specific surface areas of the zeolites. It can be concluded that the catalysis of the zeolites is related to the specific surface areas of the zeolites. After the HZSM-5/11(78) catalyst was on stream for 32 h, the surface area decreased sharply from 378 $m^2\ g^{-1}$ to 154 $m^2\ g^{-1}$, and the pore volume decreased from 0.09 $cm^3\ g^{-1}$ to 0.07 $cm^3\ g^{-1}$ whereas the pore diameter increased from 3.35 nm to 4.99 nm. This indicated that the pore structure of the HZSM-5/11(78) catalyst was blocked, being one of the reasons leading to the deactivation of the catalyst.

Table 3 Typical properties of the catalysts

Catalyst	S_{BET}[a] ($m^2\ g^{-1}$)	V[b] ($cm^3\ g^{-1}$)	d[c] (nm)	Si/Al	Total acid (μmol g^{-1})
HZSM-5(80)	338	0.15	3.61	80	222.3
HZSM-11(80)	265	0.08	7.46	80	552.2
HZSM-5/11(78)	378	0.09	3.35	78	516.4
HZSM-5/HZSM-11(80)	300	0.11	4.14	80	402.8

[a] BET surface area. [b] BJH cumulative desorption pore volume. [c] Mean pore diameter = $4V/S_{BET}$.

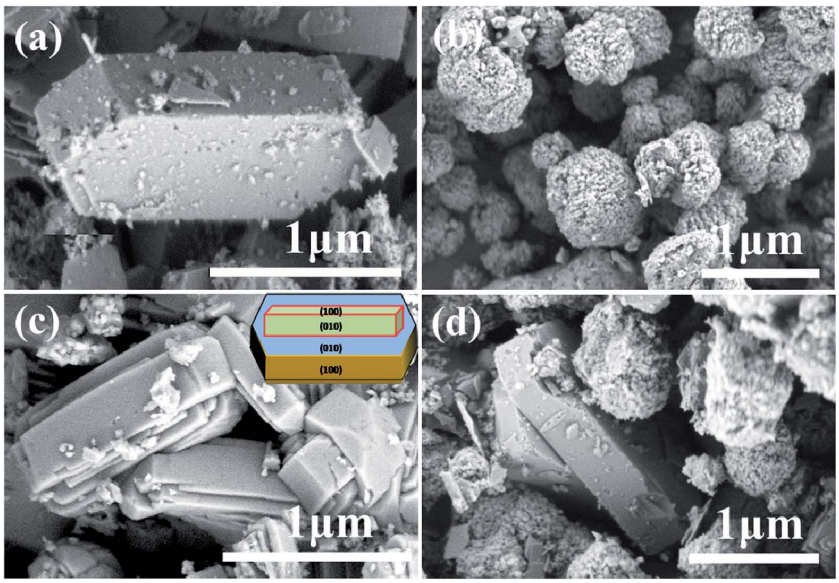

Fig. 5 SEM images for the major morphology of: (a) HZSM-5(80); (b) HZSM-11(80); (c) HZSM-5/11(78); (d) HZSM-5/HZSM-11(80).

The total acid contents of the fresh zeolites and the used HZSM-5/11(78) measured by NH_3-TPD are also shown in Table 3, and the detailed information can be found in ESI (Fig. S3A and B†). By consulting the catalytic results listed in Table 2, it can be found that the total yield of pyridine bases is not proportional to the acid contents of the zeolites. HZSM-5/11(78) with total acid contents of 516.4 μmol g^{-1}, which is between the ones of HZSM-5/HZSM-11(80) and HZSM-11(80), performed best in the catalytic conversion of glycerol to pyridine bases. HZSM-5(80) with the lowest total acid contents gave the second highest yield of pyridine bases. After the HZSM-5/11(78) catalyst was on stream for 32 h, the total acid sites of HZSM-5/11(78) decreased from 516.4 μmol g^{-1} to 282.3 μmol g^{-1}. The great decrease of the total acid sites might be ascribed to the adsorption of basic intermediates such as imines on the acid sites, which might be another reason leading to the deactivation of HZSM-5/11(78).

Our previous work[6] revealed that the co-existence of the Brønsted and Lewis acid sites in an appropriate proportion is very important in determining the total selectivity of pyridine bases. Therefore, the IR spectra of the adsorbed pyridine were employed to screen the acidity characteristics of the zeolites, and the characterization results are shown in Fig. 6A. In all the spectra the two peaks at 1450 cm^{-1} and 1545 cm^{-1} are ascribed to the absorptions of pyridine adsorbed on the Lewis and Brønsted sites of the zeolite samples, respectively.[46–48] In the spectrum of HZSM-11(80) almost no peak at 1545 cm^{-1} is observed, which indicates almost no presence of Brønsted sites in the catalyst, and the total yield of pyridine bases was only 21.2% over HZSM-11(80). However, both the peaks at 1450 cm^{-1} and 1545 cm^{-1} are displayed in the spectrum of HZSM-5(80), indicating co-existence of Lewis and Brønsted sites, and the total yield of pyridine bases over HZSM-5(80) reached to 30.4%. With mixing of HZSM-5(80) into HZSM-11(80) the concentration of Brønsted acid sites increased and a very weak peak at 1545 cm^{-1} is observed in the spectrum of HZSM-5/HZSM-11(80), and the total yield of pyridine bases over this catalyst is 27.1%. The spectrum of HZSM-5/11(78) shows high strength of the peak at 1545 cm^{-1}, and HZSM-5/11(78) gave the total yield of pyridine bases of 40.8%, which is the best of all the above catalysts. The spectra of the adsorbed pyridine in combination with the catalytic results in Table 1 indicated that both the presence of Brønsted acid sites and Lewis acid sites was essential in determining the high yields of both pyridine and 3-picoline, leading to high total yield of pyridine bases. In fact, Brønsted sites are in favor of the formation of 3-hydroxy propanal (3-HPA), from which acrolein is readily formed through a second dehydration;[49,50] by contrast, Lewis sites promote the transformation of glycerol to acetol, from its decarbonylation aldehyde is generated.[51,52] Both acrolein and aldehyde are essential in the synthesis of pyridine and 3-picoline.[5,6] Therefore, the good performance of HZSM-5/11(78) in the conversion of glycerol to pyridine bases is at least in part due to the co-existence of Brønsted acid sites and Lewis acid sites in it.

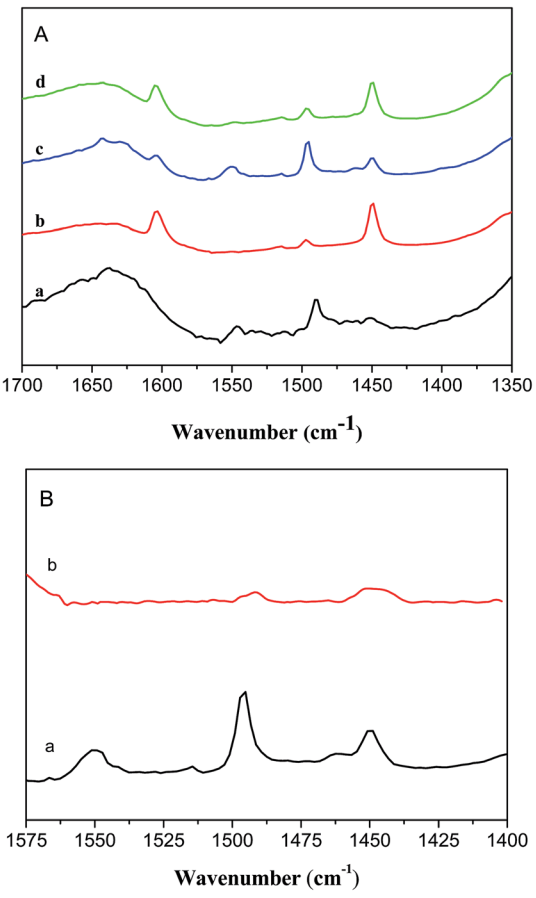

Fig. 6 (A) IR spectra of pyridine adsorbed on the catalysts. (a) HZSM-5(80); (b) HZSM-11(80); (c) HZSM-5/11(78); (d) HZSM-5(80)/HZSM-11(80). (B) IR spectra of pyridine adsorbed on the catalysts. (a) HZSM-5/11(78)(fresh); (b) HZSM-5/11(78)(used).

The spectrum of the adsorbed pyridine of the used sample of HZSM-5/11(78) was taken and compared with that of the fresh one. As shown in Fig. 6B, the peak at 1545 cm^{-1} disappeared and the strength of the peak at 1450 cm^{-1} weakened. This characterization result indicated again that some basic intermediates such as imines were adsorbed on the Brønsted sites, which led to the deactivation of the catalyst.

4. Conclusions

A composite co-crystalline zeolite HZSM-5/11(78) with a relative amount of HZSM-5 to HZSM-11 of 60 : 40 was synthesized. The HZSM-5/11(78) showed good performance in the conversion of glycerol with ammonia to pyridine bases including pyridine, 2-picoline and 3-picoline compared to zeolites with similar Si/Al ratio such as HZSM-5(80), HZSM-11(80) and the physical mixture of HZSM-5(80) and HZSM-11(80) in a similar ratio of the two components in HZSM-5/11(78). The good performance of HZSM-5/11(78) was arose from the higher surface areas and co-existence in appropriate ratio of Lewis and Brønsted sites, which are determined by the intergrowth between zeolites HZSM-5(80) and HZSM-11(80). In the catalytic conversion of glycerol with ammonia to pyridine bases, reaction temperature, molar ratio of glycerol to ammonia, GHSV and water content in the feed stocks were the major parameters influencing the reaction. Under the optimal reaction the total carbon yield of

pyridine bases reached up to 40.8% during the first 16 h of catalysis on stream, then the catalyst decreased gradually. The deactivation reasons of the catalyst could be ascribed to the deposition of substances on the catalyst leading to decrease of surface areas and pore volumes, and loss of the acid sites during catalytic run.

Acknowledgements

We acknowledge the financial support from the National Natural Science Foundation of China (Grant No. 21476057), the Natural Science Foundation of Hebei Province of China (Grant No. B2016202393, B2015202284) and the Program for the Top Young Innovative Talents of Hebei Province of China.

References

1 Y. Zheng, X. Chen and Y. Shen, *Chem. Rev.*, 2008, **108**, 5253–5277.
2 J. A. Siles Lopez, M. d. L. A. Martin Santos, A. F. Chica Perez and A. Martin Martin, *Bioresour. Technol.*, 2009, **100**, 5609–5615.
3 J. T. Dam and U. Hanefeld, *ChemSusChem*, 2011, **4**, 1017–1034.
4 Y. Zhang, T. Ma and J. Zhao, *J. Catal.*, 2014, **313**, 92–103.
5 L. Xu, Z. Han, Q. Yao, J. Deng, Y. Zhang, Y. Fu and Q. Guo, *Green Chem.*, 2015, **17**, 2426–2435.
6 Y. Zhang, X. Yan, B. Niu and J. Zhao, *Green Chem.*, 2016, **18**, 3139–3151.
7 M. Massa, A. Andersson, E. Finocchio, G. Busca, F. Lenrick and L. R. Wallenberg, *J. Catal.*, 2013, **297**, 93–109.
8 H. Atia, U. Armbruster and A. Martin, *J. Catal.*, 2008, **258**, 71–82.
9 S. H. Chai, H. P. Wang, Y. Liang and B. Q. Xu, *Appl. Catal., A*, 2009, **353**, 213–222.
10 S. Wladimir, M. Lutecki, T. Haber and H. Papp, *J. Mol. Catal. A: Chem.*, 2009, **309**, 71–78.
11 C. Jia, Y. Liu, W. Schmidt, A. Lu and F. Schüth, *J. Catal.*, 2010, **269**, 71–79.
12 F. Wang, J. L. Dubois and W. Ueda, *J. Catal.*, 2009, **268**, 260–267.
13 P. Lauriol Garbey, G. Postole, S. Loridant, A. Auroux, V. Belliere-Baca, P. Rey and J. M. M. Millet, *Appl. Catal., B*, 2011, **106**, 94–102.
14 E. Tsukuda, S. Satoshi, R. Takahashi and T. Sodesawa, *Catal. Commun.*, 2007, **8**, 1349–1353.
15 A. Chieregato, F. Basile, P. Concepción, S. Guidetti, G. Liosi, M. D. Soriano, C. Trevisanut, F. Cavani and J. M. López Nieto, *Catal. Today*, 2012, **197**, 58–65.
16 C. García-Sancho, R. Moreno-Tost, J. Mérida-Robles, J. Santamaría-González, A. Jiménez-López and P. Maireles-Torres, *Appl. Catal., A*, 2012, **433–434**, 179–187.
17 K. Omata, S. Izumi, T. Murayama and W. Ueda, *Catal. Today*, 2013, **201**, 7–11.
18 Y. Liu, H. Yang, F. Jin, Y. Zhang and Y. Li, *Chem. Eng. J.*, 2008, **136**, 282–287.
19 H. Sato, S. Shimizu, N. Abe and K. Hirose, *Chem. Lett.*, 1994, **1**, 59–62.
20 K. R. S. K. Reddy, I. Sreedhar and K. V. Raghavan, *Appl. Catal., A*, 2008, **339**, 15–20.
21 S. E. Golunski, *Appl. Catal.*, 1986, **23**, 1–14.
22 N. M. Cullinane, S. J. Chard and R. Meatyard, *J. Soc. Chem. Ind*, 1948, **67**, 142–143.
23 D. Bayramoğlu, G. Gürel, A. Sinağ and M. Güllü, *Turk. J. Chem.*, 2014, **38**, 661–670.
24 G. T. Kokotailo and N. J. Woodbury, US4289607, 1980.
25 L. Xu, J. Liu, Q. Wang, S. Liu, W. Xin and Y. Xu, *Appl. Catal., A*, 2004, **258**, 47–53.
26 L. Zhang, S. Liu, S. Xie and L. Xu, *Microporous Mesoporous Mater.*, 2012, **147**, 117–126.
27 M. Conte, B. Xu, T. E. Davies, J. K. Bartley, A. F. Carley, S. H. Taylor, K. Khalid and G. J. Hutchings, *Microporous Mesoporous Mater.*, 2012, **164**, 207–213.
28 S. Shimizu, N. Abe, A. Iguchi and H. Sato, *Catal. Surv. Jpn.*, 1998, **2**, 71–76.
29 R. Ramachandra Rao, S. J. Kulkarni, M. Subrahmanyam and A. V. Rama Rao, *React. Kinet. Catal. Lett.*, 1995, **56**, 301–309.
30 S. Shimizu, N. Abe, M. Dohba, H. Sato and K. Hirore, *Microporous Mesoporous Mater.*, 1998, **21**, 447–451.
31 X. Zhang, C. W. Luo, C. Huang and B. H. Chen, *Chem. Eng. J.*, 2014, **253**, 544–553.
32 N. Srinivas, S. J. Kulkarni and K. V. Raghavan, *Catal. Commun.*, 2002, **3**, 521–526.
33 M. Dalil, D. Carnevali, M. Edake, A. Auroux, J. L. Dubois and G. S. Patience, *J. Mol. Catal. A: Chem.*, 2016, **421**, 146–155.
34 B. Viswanadham, V. Pavankumar and K. V. R. Chary, *Catal. Lett.*, 2014, **144**, 744–755.
35 J. C. Oudejans, P. F. Van Denoosterkamp and H. Van Bekkum, *Appl. Catal.*, 1982, **3**, 109–115.
36 Y. T. Kim, K. D. Jung and E. D. Park, *Microporous Mesoporous Mater.*, 2010, **131**, 28–36.
37 P. Li, W. Zhang, X. Han and X. Bao, *Catal. Lett.*, 2010, **134**, 124–130.
38 L. Zhang, H. Liu, X. Li, S. Xe, Y. Wang, W. Xin, S. Liu and L. Xu, *Fuel Process. Technol.*, 2010, **91**, 449–455.
39 G. Gonzalez, M. E. Gomes, G. Vitale and G. R. Castro, *Microporous Mesoporous Mater.*, 2009, **121**, 26–33.
40 G. A. Jablonski, L. B. Sand and J. A. Gard, *Zeolites*, 1986, **6**, 396–402.
41 T. Q. Hoang, X. Zhu, L. L. Lobban, D. E. Resasco and R. G. Mallinson, *Catal. Commun.*, 2010, **11**, 977–981.
42 K. P. Moller, W. Bohringer, A. E. Schnitzler, E. van Steen and C. T. O'Connor, *Microporous Mesoporous Mater.*, 1999, **29**, 127–144.
43 L. Karwacki, M. H. F. Kox, D. A. Matthijs de Winter, M. R. Drury, J. D. Meeldijk, E. Stavitski, W. Schmidt, M. Mertens, P. Cubillas, N. John, A. Chan, N. Kahn, S. R. Bare, M. Anderson, J. Kornatowski and B. M. Weckhuysen, *Nat. Mater.*, 2009, **8**, 959–965.
44 M. B. J. Roeffaers, R. Ameloot, M. Baruah, H. Uji-i, M. Bulut, G. De Cremer, U. Müller, P. A. Jacobs, J. Hofkens, B. F. Sels and D. E. De Vos, *J. Am. Chem. Soc.*, 2008, **130**, 5763–5772.
45 D. L. Dorset, *Z. Kristallogr.*, 2003, **218**, 458–465.
46 C. E. Volckmar, M. Bron, U. Bentrup, A. Martin and P. Claus, *J. Catal.*, 2009, **261**, 1–8.

47 C. A. Emeis, *J. Catal.*, 1993, **141**, 347–354.
48 E. Modrogan, M. H. Valkenberg and W. F. Hoelderich, *J. Catal.*, 2009, **261**, 177–187.
49 S. H. Chai, H. P. Wang, Y. Liang and B. Q. Xu, *Green Chem.*, 2007, **9**, 1130–1136.
50 S. H. Chai, H. P. Wang, Y. Liang and B. Q. Xu, *J. Catal.*, 2007, **250**, 342–349.
51 L. G. Possato, R. N. Diniz, T. Garetto, S. H. Pulcinelli, C. V. Santilli and L. Martins, *J. Catal.*, 2013, **300**, 102–112.
52 H. Park, Y. S. Yun, T. Y. Kim, K. R. Lee, J. Baek and J. Yi, *Appl. Catal., B*, 2015, **176–177**, 1–10.